Al-implantation induced damage in 4H-SiC

Author(s):
Kumar, Piyush; Martins, Maria Inês Mendes; Prokscha, Thomas; Grossner, Ulrike

Publication date:
2024-05

Permanent link:
https://doi.org/https://doi.org/10.3929/ethz-b-000660043

Originally published in:
Materials Science in Semiconductor Processing 174, https://doi.org/10.1016/j.mssp.2024.108241

Funding acknowledgement:
- Understanding processing-induced defects to improve semiconductor device manufacturing technology ()

Materials Science in Semiconductor Processing 174 (2024) 108241

Contents lists available at ScienceDirect

Materials Science in Semiconductor Processing

journal homepage: www.elsevier.com/locate/mssp

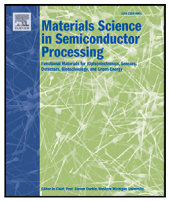

Al-implantation induced damage in 4H-SiC

P. Kumar [a,*], M.I.M. Martins [a,b], M.E. Bathen [a], T. Prokscha [b], U. Grossner [a]

[a] Advanced Power Semiconductor Laboratory, ETH Zürich, Physikstrasse 3, 8092 Zurich, Switzerland
[b] Laboratory for Muon Spin Spectroscopy, Paul Scherrer Institute, Forschungsstrasse 111, 5232 Villigen PSI, Switzerland

ARTICLE INFO

Keywords:
Al-implantation
Defects
LE-μSR
DLTS
Silicon carbide

ABSTRACT

Ion implantation of 4H-SiC is one of the crucial steps in the fabrication of power devices. This process results in the generation of electrically active defects both in the implanted region and beyond. In this work, we explore the defects created during Al-ion implantation and post implantation annealing using low-energy muon spin rotation (LE-μSR) spectroscopy and deep level transient spectroscopy (DLTS). Two sets of samples, exposed to low fluence (LF) and high fluence (HF) of Al, are examined with and without annealing. The results reveal that defects induced by Al implantation extend deep into the semiconductor, far beyond the implanted region, thus influencing the electrical properties of SiC material. The LF samples exhibit a LE-μSR signature that points to a carbon vacancy (V_C) concentration in the range of 1×10^{15} to 1×10^{19} cm^{-3}. Further, DLTS measurements reveal defect levels associated with silicon vacancies (V_{Si}) and carbon vacancies (V_C) several μm away from the intended implantation region, indicating that Al implantation and subsequent high-temperature annealing impacts the SiC lattice in a substantial volume. The present study provides valuable insights into the near-surface and bulk effects of Al implantation in 4H-SiC, which is essential for optimizing semiconductor device performance in power electronics applications.

1. Introduction

Silicon carbide (4H-SiC) is one of the most important semiconducting materials in the field of power electronics. Devices fabricated using 4H-SiC have higher power handling capability, better thermal conductivity and higher switching frequency than its silicon (Si) counterpart [1,2]. However, compared to Si, doping of SiC can be challenging due to low diffusion coefficient of dopants necessitating ion-implantation [3]. Phosphorus and nitrogen have both been employed for n-type doping in 4H-SiC, while implantation of aluminum (Al) or boron (B) can be used for creating p-doped regions. However, the relatively high ionization energy of around 0.28 eV for B, in comparison to 0.22 eV for Al, makes Al a more suitable candidate for p-type doping of 4H-SiC [4–6]. Additionally, boron impurities have been associated with lower minority carrier lifetimes in 4H-SiC epitaxial layers [7].

After implantation of dopant impurities, the samples need to be annealed at high temperatures in the range of 1600–1700 °C for electrical activation of the dopants and also to ensure good junction characteristics of the resulting device [8]. To prevent the out-diffusion of Si during high temperature annealing, the samples are usually coated with a carbon (C) cap. While ion-implantation can create vacancies and extended defects in the semiconductor, the presence of C-cap during annealing leads to injection of C into the semiconductor, resulting in a reduction of the V_C density [9] and formation of new electrically active and carbon related defects [10,11].

In SiC, implantation for p-type doping is usually required for, e.g., the creation of a termination region in Schottky barrier diodes (SBD) [12], the p^+ region in a p-n diode, or the p-body region in a metal oxide semiconductor field effect transistor (MOSFET). While the typical doping density in the p-body of a MOSFET is in the range of 1×10^{17} cm^{-3} to 1×10^{18} cm^{-3}, the p^+ region in a p–n junction device can have a doping density in the range of 1×10^{19} cm^{-3} to 1×10^{20} cm^{-3} [13]. Such high density of dopants created by ion implantation has the potential to create a high concentration of defects in the semiconductor which can have severe impact on the device performance. Deep level transient spectroscopy (DLTS) [14] is a powerful technique that is often used to study the bulk defects that are induced by ion implantation. However, the near surface information (top few hundred nanometers) is very difficult to probe using this technique. Therefore, in this study, we have carried out near surface low energy ion-implantation of Al and studied the defects created in and around the implantation region before and after high temperature annealing using low energy muon spin rotation spectroscopy (LE-μSR) [15]. To also probe the defect species created in the bulk, beyond the implanted region, DLTS measurements were performed. By conflating the results obtained from the two measurement techniques, we have built an

* Corresponding author.
E-mail address: kumar@aps.ee.ethz.ch (P. Kumar).

https://doi.org/10.1016/j.mssp.2024.108241
Received 3 January 2024; Received in revised form 5 February 2024; Accepted 12 February 2024
Available online 15 February 2024

Table 1
Sample parameters including sample name, Al fluence and whether the sample was exposed to post-implantation annealing (PIA). If yes, the sample experienced 1700 °C for 30 min.

Sample name	Fluence (cm^{-2})	PIA
LF-NotAnnealed	5×10^{13}	No
LF-Annealed	5×10^{13}	Yes
HF-NotAnnealed	5×10^{15}	No
HF-Annealed	5×10^{15}	Yes

understanding of the defect creation, migration and annihilation during Al-implantation and high temperature annealing of 4H-SiC.

2. Methodology

2.1. Sample description

For this study, n-type 4H-SiC samples with a background doping of $3{\times}10^{15}$ cm^{-3} and 10 μm epi-thickness are used. Aluminum implantation was performed at 150 keV to two different fluences in order to obtain a peak Al concentration of 10^{18} cm^{-3} or 10^{20} cm^{-3} for the two sample sets. In order to have the peak Al concentration at the surface of SiC, 275 nm of SiO_2 was deposited using plasma enhanced chemical vapor deposition (PECVD) process. After ion-implantation, the oxide was etched using hydrofluoric acid.

Each of the sample sets comprises of two samples, one of which was annealed at 1700 °C for 30 minutes after Al ion implantation, while the other was left as-implanted. The high temperature annealing was performed with a carbon cap to prevent the out-diffusion of Si during annealing. The carbon cap was later removed using an oxygen plasma. The details of the samples are summarized in Table 1.

These samples were studied using low-energy muon spin rotation (LE-μSR) spectroscopy. In a second measurement round, the top 80–90 nm of the samples was etched using an Ar-ion milling process. This allowed us to probe deeper into the sample using LE-μSR. For electrical measurements, circular Al contacts of 1.5 mm diameter and 100 nm thickness were prepared using an e-beam evaporator. The Ohmic contact on the C-face was achieved by using silver paste.

2.2. Low-energy muon spin rotation spectroscopy

The LE-μSR experiments were performed at the low-energy muon facility (LEM) located at the μE4 beamline [16] of the Swiss Muon Source at the Paul Scherrer Institute. Muons with energy ranging from 2–25 keV were implanted into the 4H-SiC epi-layers which enabled probing the first ~150 nm of the sample. For each muon implantation energy, an implantation profile is generated and the mean implanted depth of the muons can be calculated. The muon implantation profile and the calculated mean implantation depth is shown in Fig. 1. In the rest of the paper, the mean depths of the muons are used instead of the implantation energy. The measurements were carried out at 10 K and 260 K with transverse magnetic field of either 0.5 mT or 10 mT. Further details of the experiments and the analysis method can be found in Ref. [17].

The implanted muons can capture an electron from their surroundings and form the neutral paramagnetic muonium (Mu^0) state. In an n-type sample, the Mu^0 can capture another electron to form Mu^-, or in a p-type sample, capture a hole to form Mu^+, both of which are diamagnetic. In the experiments, the diamagnetic (F_D) and the paramagnetic (F_{Mu}) fraction of the muons can be measured and clearly distinguished. The muonium formation depends on the availability of free carriers, i.e., on the doping type and density. Previous experiments have also shown that the F_D (and F_{Mu}) is also sensitive to the defects present in the semiconductor and can act as a sensitive probe to local variations in the material such as defects or magnetic fields, especially for V_{Si} [18] and V_C [19] in 4H-SiC.

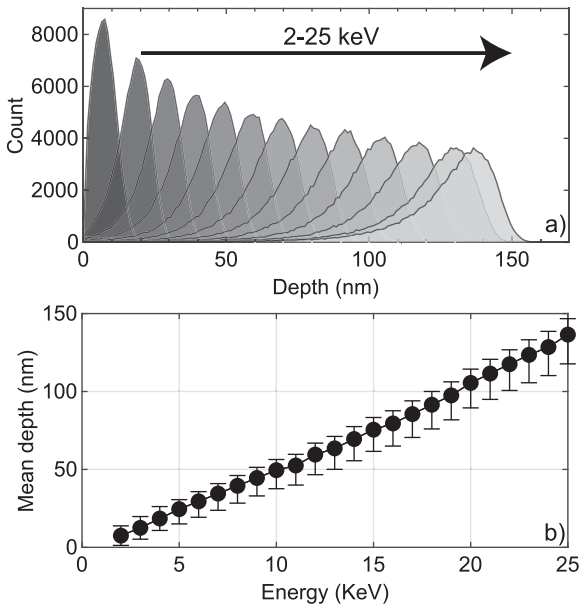

Fig. 1. (a) Muon implantation profile for energies between 2 and 25 keV, simulated with TRIM.SP [20,21]. (b) The calculated mean depth for each implantation energy is indicated with circles and the associated spread of the muon-implantation profile is indicated by the bars.

2.3. DLTS measurements

The Schottky samples were characterized using DLTS in the temperature range of 20–600 K. For DLTS, a reverse bias of −5 V is applied, and the sample is pulsed to 0 V with a pulse width of 100 ms and a period width of 500 ms. A Fourier transform of the recorded transients is performed using up to 28 correlation functions. The DLTS signal shown in the rest of the paper refers to the coefficient of the sine term (b1) in the Fourier series of the deep level transient Fourier spectroscopy (DLTFS) [22].

3. Results

Implantation of Al in 4H-SiC is known to create damage in the crystal leading to the formation of several deep level defects [23]. High-temperature post implantation annealing (PIA) is commonly employed to restore the implantation induced damage and for the electrical activation of Al. However, to prevent out-diffusion of Si during the PIA, a carbon cap is prepared on the surface of SiC. This may result in C-injection, leading to the emergence of various defects related to carbon interstitials (C_i) in the sample.

3.1. LE-μSR study

LE-μSR measurements were performed on the Al-implanted samples to study the defects created by implantation and high temperature annealing. In this experiment, the muons are not expected to interact with the implanted Al, but rather with the intrinsic point defects present in the sample as a result of processing (ion implantation and high-temperature PIA with C-cap). Fig. 2 shows the diamagnetic fraction measured for the low fluence and the high fluence samples as a function of depth at 10 K and 260 K. For the low-fluence sample before annealing (Fig. 2(a), a high F_D is recorded near the surface and it drops as the muons penetrate deeper into the sample. The μSR measurement was performed up to a mean depth of ~140 nm, and it can be seen that the F_D is reduced almost fourfold from the surface until 140 nm depth. Further, the F_D value measured at 10 K is higher than the measurement at 260 K in the entire depth. This is opposite to what was observed

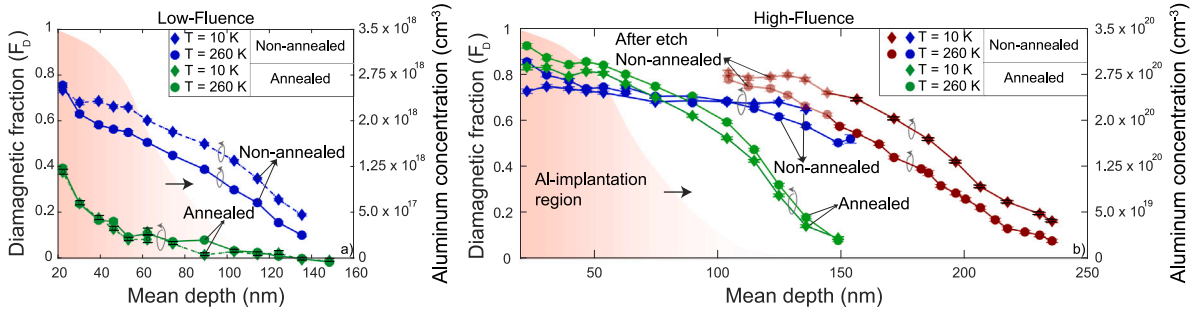

Fig. 2. Diamagnetic fraction recorded at a magnetic field 10 mT as a function of mean depth for the (a) LF-NotAnnealed and LF-Annealed samples, and (b) HF-NotAnnealed and HF-Annealed samples. The shaded regions in both the graphs indicate the Al-implantation region, and the expected Al-concentration is indicated on the right. For the HF-NotAnnealed sample, another LE-μSR measurement was performed after etching the top 80 nm of the sample as indicated in (b).

in Ref. [24], where the F_D increased with increasing temperature due to the availability of more carriers. However, in Ref. [19], proton irradiated samples were studied using LE-μSR and it was observed that the F_D was higher at 5 K than at 200 K, similar to the current case. Since the samples have a background n-type doping of $3 \times 10^{15}\,cm^{-3}$, a compensation of carriers is expected due to high concentration of implantation induced defects.

After annealing, the implantation induced damage is reduced and a substantial drop in F_D is observed for the LF-Annealed sample near the surface (see (Fig. 2(a). At a depth of around 60 nm, the F_D drops to the bulk level. Almost no temperature dependence is observed in the low fluence annealed sample. However, a higher F_D near the surface compared to at ~80 nm depth indicates that either a part of the implantation induced damage persists after high temperature annealing, or the C-related defects formed due to C-injection during PIA leads to an increase in the F_D.

Fig. 2(b) shows the F_D measured for the HF-Annealed and HF-NotAnnealed sample. Similar to the low fluence case, a high F_D is observed near the surface for the not-annealed sample. However, for the high fluence Al implantation without PIA, the diamagnetic fraction does not drop substantially for the first ~150 nm of the sample. This indicates a high concentration of defects extending from the surface up to 150 nm in the sample. Since the probing depth is limited to ~150 nm at the LE-μSR setup, the muon response in the regions deeper into the sample could not be directly extracted. To overcome this, we etched the top 80 nm of the sample (see sample description) and re-measured the sample with LE-μSR. Although a small increase in the F_D was observed in the first 50 nm after the etch when compared to the previous measurement (attributed to Ar milling induced damage), the F_D gradually drops and reaches the bulk level at around 240 nm depth. This measurement reveals that the defects created during the implantation extend up to ~240 nm into the sample. This is deeper than the Al implantation region (0 nm to 100 nm) by over 140 nm.

Fig. 2(b) also shows the F_D measured for the HF-Annealed sample. Compared to the not-annealed sample, a small increase in F_D is observed near the surface at 260 K (attributed to the electrical activation of Al and resulting presence of holes), but the values drop quickly for higher muon energies that travel deeper into the sample. At around 150 nm, the F_D has dropped from > 0.9 near the surface to < 0.1. This indicates a substantial reduction in defect concentration due to post implantation anneal (PIA) along with the electrical activation of dopants leading to an increase in F_D with increasing temperature. However, in the first ~80 nm for the HF-Annealed sample, the F_D is slightly higher than the HF-NotAnnealed sample. As at 10 K, no carriers are expected to be present in the sample, the relatively high diamagnetic fraction measured for the HF-Annealed sample near the surface can be attributed to incomplete restoration of crystal damage during the PIA or due to the high density of injected C species from the C-cap.

In order to understand the relation between the measured F_D and the defects generated during ion-implantation, we have carried out

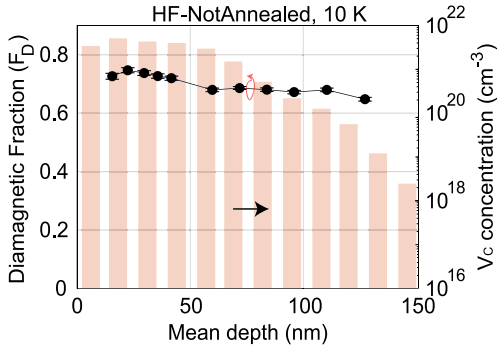

Fig. 3. The diamagnetic fraction of the HF-NotAnnealed sample is plotted. The V_C concentration extracted from the SRIM simulation is also plotted for the high fluence samples. A good agreement between the trend of F_D and defect concentration is observed.

SRIM simulations [25]. The simulation was performed for the layered stack of bulk 4H-SiC and 275 nm of SiO_2. 150 keV Al ions were implanted in the simulation. The carbon vacancy (V_C) and silicon vacancy (V_{Si}) concentration profiles were obtained assuming a 3 % dynamic annealing survival rate [26]. Figs. 3 and 4 show the V_C concentration obtained for a high and low fluence of Al implantation prior to PIA. The V_C concentration shown in the two figures is therefore 3 % of the total defects obtained from SRIM simulation. The F_D obtained for the LF- and HF-NotAnnealed samples at 10 K, respectively, are overlaid on the V_C defect profile for comparison. The F_D for both the samples is close to 0.75 near the surface although the two samples have two orders of magnitude difference in the defect concentration. This shows an upper limit of around $1 \times 10^{19}\,cm^{-3}$ for the sensitivity of muons to the V_C concentration in the LE-μSR measurement. For the LF-NotAnnealed sample, the F_D drops with the depth and has almost the same trend as the defect concentration profile. Another measurement was performed on the LF-NotAnnealed sample after the first 80 nm was etched and the result is shown in Fig. 4. Apart from an increase in F_D in the first ~ 30 nm of the measured region which is attributed to Ar-ion milling induced damage, the trend between the V_C concentration and F_D aligns very well. The F_D reaches almost 0 for a C vacancy concentration $<1 \times 10^{15}\,cm^{-3}$. The strong correlation between the measured F_D and the defect concentration confirms the sensitivity of muons to the carbon vacancies that are present in our samples and helps us establish that the LE-μSR experiment is sensitive to a carbon vacancy concentration in the range of $1 \times 10^{15}\,cm^{-3}$ to $1 \times 10^{19}\,cm^{-3}$. The F_D signal measured at 10 K in this defect range is from ~0 to 0.6 with an increment of 0.15 per decade.

Along with the V_C, silicon vacancies are also generated during Al ion-implantation and have a similar profile to the V_C but at around half the concentration. Presence of V_{Si} is expected to reduce the measured

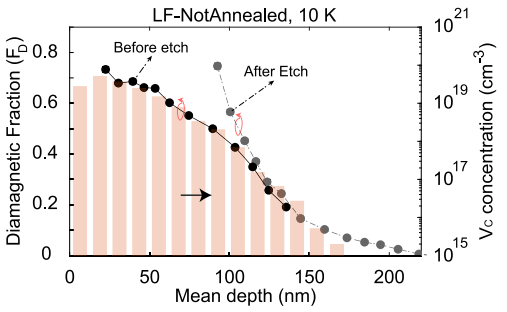

Fig. 4. The diamagnetic fraction of the LF-NotAnnealed sample at 10 K and 10 mT is shown. The top ~80 nm of the sample was then etched and a second measurement was performed indicated as 'After Etch'. The concentration of V_C after Al-implantation was simulated using SRIM and is plotted for comparison. good agreement between the trend of F_D and defect concentration is observed.

F_D [18]. As seen in Fig. 2(a) for the LF-NotAnnealed sample and in Fig. 2(b) for the HF-NotAnnealed sample, the measured F_D is reduced at 260 K in comparison to at 10 K. This could be an ensemble effect of the two defect species (V_C and V_{Si}) where the impact of V_C is dominant on the μSR signal at low temperature, while the V_{Si} begins to reduce the F_D as the temperature increases.

3.2. Bulk damage

The μSR measurements demonstrate the presence of defective regions in the SiC after Al-implantation and PIA in the top ~200 nm, but not deeper in the SiC bulk. Due to the limitation of probing depth and sensitivity, LE-μSR cannot be used for characterization until micrometer depths and in regions with reduced densities of defects. Therefore, we have used DLTS to study the defects created in the bulk of the semiconductor by Al implantation and PIA. The DLTS spectra and the depth profiles for the electrically active defects that are observed in the four samples are shown in Figs. 5 and 6. The extracted parameters of the defects for the four samples are summarized in Table 2.

For the LF-NotAnnealed sample, shown in Fig. 5(a), five defect levels are visible in the measured range of 80–600 K and named as IN1, IN3, IN4, IN5, and IN6. The nomenclature for the observed defects has been adapted from Ref. [23]. The spectrum of the reference sample without any processing is also plotted for comparison (black curve). The IN1 defect is only barely visible and has an activation energy (E_A) of 0.4 eV and a capture cross section (CCS) of 2.1×10^{-15} cm^2. This corresponds closely to the S1 level assigned to the (2-/3-) charge transition level (CTL) of the silicon vacancy (V_{Si}) defect [26–29]. The IN4 level has an E_A of 0.71 eV and a CCS of 1.2×10^{-15} cm^2 and likely corresponds to the S2 level associated with V_{Si}(-/2-). The IN3 level aligns well with the defect observed in the reference spectrum and has an E_A of 0.67 eV and a CCS of 7×10^{-15} cm^2. This defect likely belongs to the carbon vacancy (V_C) and is usually named $Z_{1/2}$ [30,31]. The IN5 and IN6 defect levels have E_A of 0.8 eV and 1.01 eV, respectively. These values are very close to what has been observed after C-ion implantation [32] and after thermal oxidation [11,33,34] and are assumed to be associated with C_i related defects consisting of one or more C atoms. The commonly used names for IN5 and IN6 are ON1 and ON2a, respectively.

The depth profiles measured for the IN4, IN5 and IN6 defect levels after low-fluence Al implantation but before PIA are shown in Fig. 5(b). An exponential fit was created for each of the depth profiles and is shown with dotted lines in the figure, which allows for extrapolation of the defect concentration towards the surface. As can be seen, a high defect concentration in the range of 1×10^{15} cm^{-3} to 1×10^{16} cm^{-3} for all probed defects (IN4-IN) is expected at a depth of 0.5 µm from the surface.

Upon annealing the sample at 1700° for 30 minutes, the implanted Al is expected to be activated and some of the crystal damage is restored. However, since the annealing is performed with a C-cap to prevent out-diffusion of Si atoms and reduced surface roughness [35], C-injection is expected which can result in several new defect levels [10]. The DLTS spectrum of the LF-Annealed sample is illustrated in Fig. 5(c). The first thing to note is the presence of a minority carrier trap (INo2) in the DLTS spectrum. This is usually due to injection of minority carriers during the DLTS transient. Since Al was implanted into the sample and the sample was annealed at elevated temperatures, Al is electrically activated and acts as a source of minority carriers. The E_A calculated for this defect is 0.25 eV with a capture cross section of 2.6×10^{-17} cm^{-2}. This defect could likely be due to boron (B) on Si

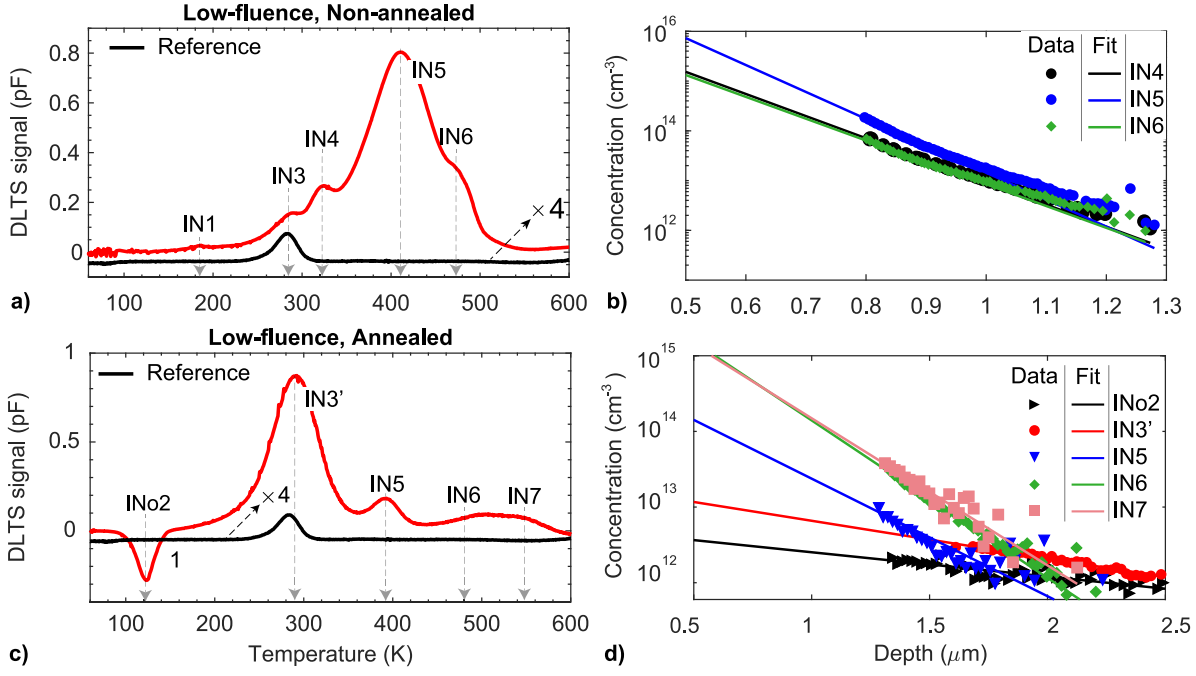

Fig. 5. The DLTS spectra and the depth profiles of the observed defects are plotted in (a)–(b) for LF-NotAnnealed sample and in (c)–(d) for LF-Annealed sample.

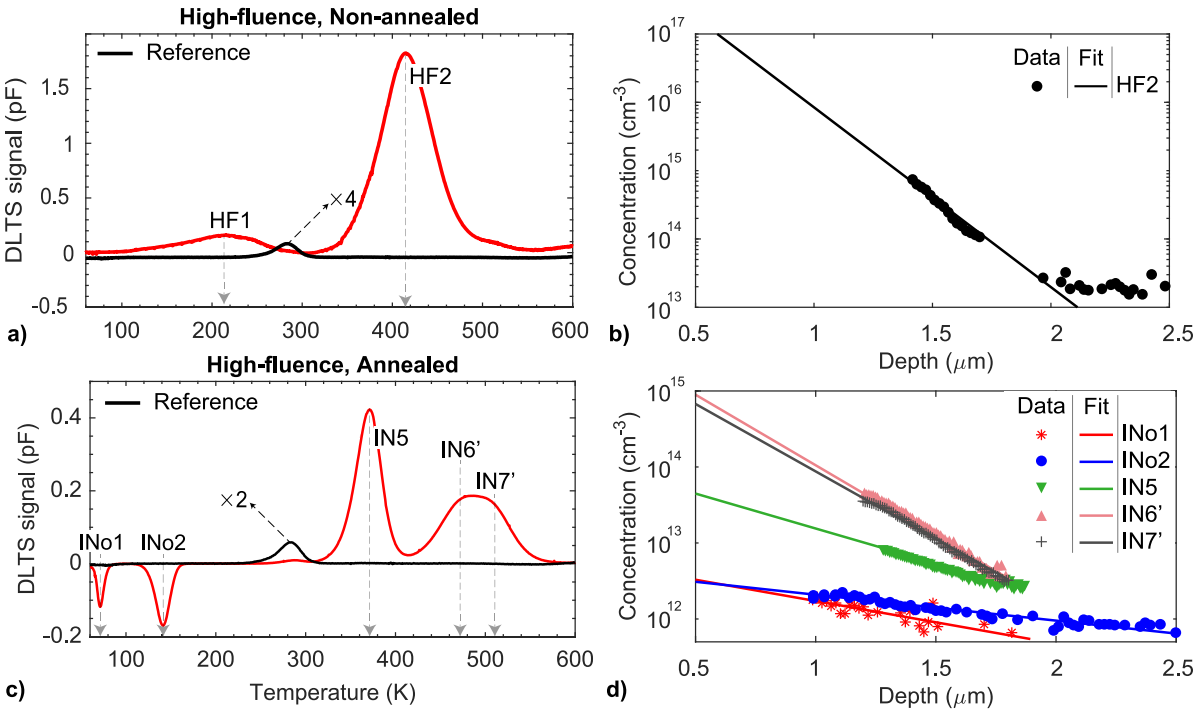

Fig. 6. The DLTS spectra and the depth profiles of the observed defects are plotted in (a)–(b) for HF-NotAnnealed sample and in (c)–(d) for HF-Annealed sample.

Table 2
Summary of the defects observed in the Al implanted and annealed samples, including energy level above the valence band edge (top table) or below the conduction band edge (bottom table), measured (σ) capture cross-section (cm^2), and whether the defect species was observed in the sample or not.

Name	Energy (eV)	σ (cm^2)	LF-NotAnnealed	LF-Annealed	HF-NotAnnealed	HF-Annealed
INo1	0.18	2.1×10^{-15}	–	–	–	Observed
INo2	0.25	2.6×10^{-17}	–	Observed	–	Observed
IN_1	0.4	2.1×10^{-15}	Observed	–	–	–
IN_3	0.67	7×10^{-15}	Observed	–	–	–
IN_4	0.71	1.2×10^{-15}	Observed	–	–	–
IN_5	0.8	4.8×10^{-17}	Observed	Observed	–	Observed
IN_6	1.05	2.5×10^{-16}	Observed	Observed	–	Observed
IN_7	1.17	2.9×10^{-16}	–	Observed	–	Observed

site introduced in the epitaxial layer during chemical vapor deposition growth process [7,36,37].

The second defect level (IN3') observed in the LF-Annealed sample aligns well with the $Z_{1/2}$ level observed in the reference sample. During PIA at 1700°C with a C-cap, we expect generation of V_C and C_is due to the high temperature as well as the injection of C_is from the surface. However, due to the high formation energy of V_C is ~5 eV [38], relatively low concentrations (1×10^{11} cm^{-3} to 1×10^{12} cm^{-3}) of carbon vacancy and interstitial generation is expected. Simultaneously, we have C-injection from the C-cap at the surface, which could annihilate with V_C [9] resulting in the reduction of carbon vacancy related defects. Overall we expect high concentration of C_i and its complexes in the sample. The Arrhenius analysis for the IN3' defect level results in a poor fit with very low correlation, and therefore a fitting approach has been employed to extract the defect parameters. Four defect levels were identified to be associated with the IN3' level which have activation energies ranging between 0.42–0.51 eV. Therefore, it is possible that the IN3' level may not be due to the carbon vacancies. At the same time, the V_{Si} is also expected to anneal out during the 1700 °C PIA [39], resulting in the reduction of its concentration. Therefore, the defect levels observed for IN3' are likely C-interstitial related. The IN5, IN6 and IN7 defect levels have activation energies of 0.8 eV, 1.05 eV and 1.17 eV, respectively. Similar to the LF-NotAnnealed sample, these values are close to what has been observed previously and are assumed to be associated with C_i related defects consisting of one or more C atoms. While IN5 and IN6 are referred to as ON1 and ON2a respectively, the IN7 level is usually referred to as ON2b.

The depth profiles and the corresponding exponential fits for the defects observed after low fluence Al-implantation and PIA are illustrated in Fig. 5 d). The defect concentration could be measured up to 2.5 μm depth which is a significant increase from the 1.2 μm extension that was found for the IN4, IN5 and IN6 defects right after low-fluence implantation (see Fig. 5b). This highlights the mobile nature of C_i related defects which can migrate deep into the sample at elevated temperatures. Furthermore, apart from the concentration profile of the INo2 defect level which appears to change only very slightly in the measured range, the rest of the levels decay exponentially. The exponential extrapolation of the IN5, IN6 and IN7 defect levels in Fig. 5 d) suggests an expected concentration in the range of 1×10^{14} cm^{-3} to 1×10^{16} cm^{-3} at a depth of 0.5 μm from the surface.

Fig. 6(a) shows the DLTS spectrum of the HF-NotAnnealed sample. Two broad peaks are observed in the spectrum (labeled HF1 and HF2) and could not be studied with an Arrhenius analysis. A fitting approach was chosen to deconvolute the defect signatures contributing to the spectrum and it was found that up to 8 defect levels ranging from 0.19–0.38 eV were needed to reproduce the HF1 level while 4 levels ranging from 0.75–0.9 eV are required to reproduce HF2. This suggests a high degree of damage created in the sample after high fluence Al-implantation. The depth profile obtained from the isothermal DLTS

measurement at the peak temperature of the HF2 level is shown in Fig. 6(b). A defect concentration larger than $1 \times 10^{13}\,cm^{-3}$ is observed at a depth of 2.5 μm while the exponential extrapolation suggests a concentration of defects higher than $1 \times 10^{17}\,cm^{-3}$ at a depth of 0.5 μm from the surface.

Upon PIA, a significant change in the spectrum is observed as shown in Fig. 6(c). Similar to the LF-Annealed sample, the INo2 level is observed which corresponds to B on the Si site. However, a new minority trap level (INo1) is observed and has an E_A of 0.18 eV and a CCS of $2.1 \times 10^{-15}\,cm^2$. This E_A value for INo1 is close to the observed X-peak after heavy ion irradiation [40] and could be due to Al acceptor level on Si site [41]. Detailed study on the INo1 (X peak) is being carried out and shall be presented in Ref. [11]. Three other defect levels which appear in the spectrum are IN5, IN6' and IN7'. IN5 has similar properties as those observed in the LF-Annealed sample, whereas the IN6' and IN7' levels appear to have slightly reduced (by ~0.1 eV) activation energies as compared to their IN6/IN7 counterparts. However, apart from the additional IN3 defect level observed in the LF-Annealed sample, similar majority carrier traps are observed in the HF-Annealed sample as well. The depth profiles associated with the observed defect levels are shown in Fig. 6 d). IN5, IN6' and IN7' show similar behavior in their depth profiles as was observed in the LF-Annealed sample.

4. Discussion

Implanted Al in 4H-SiC at 150 keV is expected to collide with C and Si atoms in the lattice and create vacancies (V_C, V_{Si}) and interstitials (C_i, Si_i) in the process. Displacement energies of Si and C atoms are expected in the range of 20–30 eV [42,43]. However, due to the difference in mass of Si and C atoms ($M_{Si}/M_C = 2.33$), the energy required of the impinging particle to displace C atoms is smaller than for the Si atoms. In case of Al implantation at 150 keV, both C and Si vacancies can be generated, however, based on SRIM simulations the concentration of V_{Si} is expected to be almost half of that of the V_C concentration. As shown in Ref. [18,19], the F_D measured in the LE-μSR experiment is sensitive to the presence of both V_{Si} and V_C, where F_D increases with increasing V_C concentration whereas it reduces with increasing V_{Si} concentration. However, as shown above, at a low temperature of 10 K, the LE-μSR signal is very sensitive to the V_C concentration showing a strong correlation between the measured F_D and the simulated V_C concentration (Fig. 4).

Along with the vacancies, interstitials are also generated during implantation, namely the Si and C interstitials (Si_i, C_i). The C_i are highly mobile with a small migration barrier of ~2 eV and can migrate up to a micron [39] after implantation. This is confirmed by the DLTS spectrum and the depth profile of the LF-NotAnnealed sample illustrated in Fig. 5(a) and (b). The IN5 and IN6 defects are likely caused due to different complexes of the C_i. However, the V_{Si} (IN1, IN4) and V_C (IN3) are also observed in the spectrum which suggests that these point defects are also able to migrate up to a micron into the sample under the non-equilibrium conditions during Al-implantation. In the HF-NotAnnealed sample, with 100 times higher fluence of Al than the LF-NotAnnealed sample, significantly higher concentration of vacancies and interstitials are generated. The F_D is almost flat (Fig. 2(b)) in the implanted region which is likely due to the very high concentration of V_C well above the sensitivity limit of LE-μSR experiment. Simultaneously, the DLTS spectrum consists of broad peaks comprising of several closely spaced defect species likely formed due to different complexes of C_i.

PIA at 1700°C results in the activation of dopants as confirmed by the increase in F_D at 260 K in comparison to at 10 K (Fig. 2(b) and the presence of the minority trap levels in the DLTS signal of both the LF- and HF-Annealed samples. In addition, the PIA is also expected to restore crystal damage which is likely the case beyond the first 100 nm of the sample due to the reduction of the F_D observed in Fig. 2(a) and 2b). However, in the first ~80 nm for the HF-Annealed sample, the F_D remains almost the same at 10 K, before and after annealing. As at 10 K no carriers are expected to be present in the sample, the high diamagnetic fraction measured can be attributed to incomplete restoration of crystal damage during the PIA or due to the high density of injected C related species. Further, PIA also leads to the generation of V_C+C_i pair in low concentration, migration of the existing defect species and injection of C_is from the C-cap. The C_is created during implantation and injected C_i can annihilate with the existing V_C, significantly reducing the V_C concentration [9,44]. This is confirmed by the absence of the IN3 defect center in the LF and HF-Annealed samples. However, since large quantities of C_is are injected into the sample, several stable defect species that have been assigned to C related defects arise in the DLTS spectrum (IN5, IN6 and IN7) and are found herein to extend up to 2 μm in the sample.

5. Conclusion

In this work, the impact of Al implantation and post implantation annealing on 4H-SiC is studied. The surface and near surface region of up to 200 nm is studied with nanometer depth resolution using LE-μSR while the bulk extending up to a few micrometers was studied with DLTS. We have observed that LE-μSR can be a very powerful method to perform a depth resolved study of the defects created during implantation and post implantation annealing. The generated carbon vacancies during implantation result in an increase in the diamagnetic fraction (F_D) of the muons, allowing the possibility to establish a direct correlation between the F_D and the V_C concentration. LE-μSR can therefore be very helpful to study the near surface region of a sample with high defect sensitivity.

DLTS measurements performed on the not-annealed samples reveal the presence of V_C and V_{Si} at a depth of around 1 μm along with several C_i related defect species immediately after Al implantation. After the high temperature anneal, V_C and V_{Si} are not observed in the DLTS measurements due to possible annihilation with injected C_is. However, several defect levels that are assigned to C_i and its complexes are observed, which extend up to a depth of 2-2.5 μm in the semiconductor.

With the sensitivity range offered by LE-μSR and DLTS combined, defect densities from $1 \times 10^{11}\,cm^{-3}$ to $1 \times 10^{19}\,cm^{-3}$ can be studied. Simultaneously, the near surface region which is challenging to probe with DLTS can be studied in high resolution using LE-μSR, whereas the deeper regions that are unavailable with LE-μSR can be probed precisely with DLTS. Therefore, the two characterization methods used in this work complement each other well and enable a comprehensive study of the impact of Al implantation on the semiconductor and defect parameters that directly influence power device performance.

CRediT authorship contribution statement

P. Kumar: Writing – original draft, Visualization, Validation, Project administration, Investigation, Formal analysis, Conceptualization. **M.I.M. Martins:** Writing – review & editing, Investigation, Formal analysis, Conceptualization. **M.E. Bathen:** Writing – original draft, Supervision, Investigation, Conceptualization. **T. Prokscha:** Writing – review & editing, Supervision, Resources, Funding acquisition, Conceptualization. **U. Grossner:** Writing – review & editing, Supervision, Resources, Funding acquisition, Conceptualization.

Declaration of competing interest

The authors declare that they have no known competing financial interests or personal relationships that could have appeared to influence the work reported in this paper.

Data availability

Data will be made available on request.

Acknowledgments

The muon experiments were performed at the μE4/LEM beamline of the Swiss Muon Source SμS, Paul Scherrer Institute, Villigen, Switzerland. This work is supported by the Swiss National Science Foundation under the Grant No. 192218. The work of MEB was supported by an ETH Zürich Postdoctoral Fellowship, Switzerland.

References

[1] A. Ong, J. Carr, J. Balda, A. Mantooth, A comparison of silicon and silicon carbide MOSFET switching characteristics, in: 2007 IEEE Region 5 Technical Conference, 2007, pp. 273–277, http://dx.doi.org/10.1109/TPSD.2007.4380318, URL: https://ieeexplore.ieee.org/document/4380318.

[2] J. Wang, A comparison between Si and SiC MOSFETs, IOP Conf. Ser. Mater. Sci. Eng. 729 (1) (2020) 012005, http://dx.doi.org/10.1088/1757-899X/729/1/012005, URL: https://iopscience.iop.org/article/10.1088/1757-899X/729/1/012005.

[3] J.D. Hong, R.F. Davis, D.E. Newbury, Self-diffusion of silicon-30 in α-SiC single crystals, J. Mater. Sci. 16 (9) (1981) 2485–2494, http://dx.doi.org/10.1007/BF01113585.

[4] Y. Negoro, T. Kimoto, H. Matsunami, F. Schmid, G. Pensl, Electrical activation of high-concentration aluminum implanted in 4H-SiC, J. Appl. Phys. 96 (9) (2004) 4916–4922, http://dx.doi.org/10.1063/1.1796518, URL: https://pubs.aip.org/jap/article/96/9/4916/954368/Electrical-activation-of-high-concentration.

[5] L. Lu, H. Zhang, X. Wu, J. Shi, Y.Y. Sun, Atomic and electronic structures of p-type dopants in 4H-SiC, Chin. Phys. B 30 (9) (2021) 096806, http://dx.doi.org/10.1088/1674-1056/ac1e22, URL: https://iopscience.iop.org/article/10.1088/1674-1056/ac1e22.

[6] I. Capan, T. Brodar, Y. Yamazaki, Y. Oki, T. Ohshima, Y. Chiba, Y. Hijikata, L. Snoj, V. Radulović, Influence of neutron radiation on majority and minority carrier traps in n-type 4H-SiC, Nucl. Instrum. Methods Phys. Res. B 478 (2020) 224–228, http://dx.doi.org/10.1016/j.nimb.2020.07.005, URL: https://linkinghub.elsevier.com/retrieve/pii/S0168583X20303359.

[7] M. Ghezellou, P. Kumar, M.E. Bathen, R. Karsthof, E.Ö. Sveinbjörnsson, U. Grossner, J.P. Bergman, L. Vines, J. Ul-Hassan, The role of boron related defects in limiting charge carrier lifetime in 4H–SiC epitaxial layers, APL Mater. 11 (3) (2023) 031107, http://dx.doi.org/10.1063/5.0142415.

[8] T. Kimoto, O. Takemura, H. Matsunami, T. Nakata, M. Inoue, Al+ and B+ implantations into 6H-SiC epilayers and application to pn junction diodes, J. Electron. Mater. 27 (4) (1998) 358–364, http://dx.doi.org/10.1007/s11664-998-0415-6.

[9] H.M. Ayedh, R. Nipoti, A. Hallén, B.G. Svensson, Thermodynamic equilibration of the carbon vacancy in 4H-SiC: A lifetime limiting defect, J. Appl. Phys. 122 (2) (2017) 025701, http://dx.doi.org/10.1063/1.4991815, URL: http://aip.scitation.org/doi/10.1063/1.4991815.

[10] R. Karsthof, M.E. Bathen, A. Kuznetsov, L. Vines, Formation of carbon interstitial-related defect levels by thermal injection of carbon into n-type 4H-SiC, J. Appl. Phys. 131 (3) (2022) 035702, http://dx.doi.org/10.1063/5.0077308, URL: http://arxiv.org/abs/2111.01011, arXiv:2111.01011 [cond-mat, physics:physics].

[11] M.E. Bathen, P. Kumar, M. Ghezellou, M. Belanche, L. Vines, U. Grossner, Dual configuration of shallow acceptor levels in 4H-SiC, 2024, Submitted.

[12] Sang-Cheol Kim, Wook Bahng, In-Ho Kang, Sung-Jae Joo, Nam-Kyun Kim, Fabrication characteristics of 1.2kv SiC JBS diode, in: 2008 26th International Conference on Microelectronics, IEEE, Nis, Serbia and Montenegro, 2008, pp. 181–184, http://dx.doi.org/10.1109/ICMEL.2008.4559253, URL: http://ieeexplore.ieee.org/document/4559253/.

[13] T. Kimoto, J.A. Cooper, Fundamentals of Silicon Carbide Technology: Growth, Characterization, Devices, and Applications, John Wiley & Sons Singapore Pte. Ltd, Singapore, 2014, http://dx.doi.org/10.1002/9781118313534, URL: http://doi.wiley.com/10.1002/9781118313534.

[14] D.V. Lang, Deep-level transient spectroscopy: A new method to characterize traps in semiconductors, J. Appl. Phys. 45 (7) (1974) 3023–3032, http://dx.doi.org/10.1063/1.1663719, URL: https://pubs.aip.org/jap/article/45/7/3023/6845/Deep-level-transient-spectroscopy-A-new-method-to.

[15] E. Morenzoni, H. Glu, T.J. Jackson, H. Luetkens, C. Niedermayer, M. Pleines, M. Birke, A. Hofer, J. Litterst, T. Riseman, G. Schatz, Low-energy SR at PSI: present and future, Physica B (2000).

[16] T. Prokscha, E. Morenzoni, K. Deiters, F. Foroughi, D. George, R. Kobler, A. Suter, V. Vrankovic, The new μE4 beam at PSI: A hybrid-type large acceptance channel for the generation of a high intensity surface-muon beam, Nucl. Instrum. Methods Phys. Res. A 595 (2) (2008) 317–331, http://dx.doi.org/10.1016/j.nima.2008.07.081, URL: https://www.sciencedirect.com/science/article/pii/S016890020801067X.

[17] M. Mendes Martins, P. Kumar, J. Woerle, X. Ni, U. Grossner, T. Prokscha, Defect profiling of oxide-semiconductor interfaces using low-energy muons, Adv. Mater. Interfaces 2300209, http://dx.doi.org/10.1002/admi.202300209, URL: https://onlinelibrary.wiley.com/doi/abs/10.1002/admi.202300209.

[18] J. Woerle, M. Bathen, T. Prokscha, A. Galeckas, H. Ayedh, L. Vines, U. Grossner, Muon interaction with negative- U and high-spin-state defects: Differentiating between C and Si vacancies in 4 H - Si C, Phys. Rev. A 14 (5) (2020) 054053, http://dx.doi.org/10.1103/PhysRevApplied.14.054053, URL: https://link.aps.org/doi/10.1103/PhysRevApplied.14.054053.

[19] J. Woerle, T. Prokscha, A. Hallén, U. Grossner, Interaction of low-energy muons with defect profiles in proton-irradiated Si and 4 H -SiC, Phys. Rev. B 100 (11) (2019) 115202, http://dx.doi.org/10.1103/PhysRevB.100.115202, URL: https://link.aps.org/doi/10.1103/PhysRevB.100.115202.

[20] E. Morenzoni, H. Glückler, T. Prokscha, R. Khasanov, H. Luetkens, M. Birke, E.M. Forgan, C. Niedermayer, M. Pleines, Implantation studies of kev positive muons in thin metallic layers, Nucl. Instrum. Methods Phys. Res. B 192 (3) (2002) 254–266, http://dx.doi.org/10.1016/S0168-583X(01)01166-1, URL: https://www.sciencedirect.com/science/article/pii/S0168583X01011661.

[21] W. Eckstein, in: U. Gonser, A. Mooradian, R.M. Osgood, M.B. Panish, H. Sakaki, H.K.V. Lotsch (Eds.), Computer Simulation of Ion-Solid Interactions, in: Springer Series in Materials Science, vol. 10, Springer, Berlin, Heidelberg, 1991, http://dx.doi.org/10.1007/978-3-642-73513-4, URL: https://link.springer.com/10.1007/978-3-642-73513-4.

[22] S. Weiss, R. Kassing, Deep level transient Fourier spectroscopy (DLTFS)—A technique for the analysis of deep level properties, Solid-State Electron. 31 (12) (1988) 1733–1742, http://dx.doi.org/10.1016/0038-1101(88)90071-8, URL: https://linkinghub.elsevier.com/retrieve/pii/0038110188900718.

[23] K. Kawahara, G. Alfieri, T. Kimoto, Detection and depth analyses of deep levels generated by ion implantation in n- and p-type 4H-SiC, J. Appl. Phys. 106 (1) (2009) 013719, http://dx.doi.org/10.1063/1.3159901, URL: https://pubs.aip.org/jap/article/106/1/013719/396870/Detection-and-depth-analyses-of-deep-levels.

[24] P. Kumar, M.I.M. Martins, M.E. Bathen, J. Woerle, T. Prokscha, U. Grossner, Investigation of the Si O 2 - Si C interface using low-energy muon-spin-rotation spectroscopy, Phys. Rev. A 19 (5) (2023) 054025, http://dx.doi.org/10.1103/PhysRevApplied.19.054025, URL: https://link.aps.org/doi/10.1103/PhysRevApplied.19.054025.

[25] J.F. Ziegler, SRIM-2003, Nucl. Instrum. Methods Phys. Res. B 219–220 (2004) 1027–1036, http://dx.doi.org/10.1016/j.nimb.2004.01.208, URL: https://www.sciencedirect.com/science/article/pii/S0168583X04002587.

[26] M.E. Bathen, A. Galeckas, J. Müting, H.M. Ayedh, U. Grossner, J. Coutinho, Y.K. Frodason, L. Vines, Electrical charge state identification and control for the silicon vacancy in 4H-SiC, npj Quantum Inf. 5 (1) (2019) 111, http://dx.doi.org/10.1038/s41534-019-0227-y, URL: http://www.nature.com/articles/s41534-019-0227-y.

[27] M.L. David, G. Alfieri, E.M. Monakhov, A. Hallén, C. Blanchard, B.G. Svensson, J.F. Barbot, Electrically active defects in irradiated 4H-SiC, J. Appl. Phys. 95 (9) (2004) 4728–4733, http://dx.doi.org/10.1063/1.1689731, URL: http://aip.scitation.org/doi/10.1063/1.1689731.

[28] P. Kumar, M. Belanche, N. Für, L. Guzenko, J. Woerle, M.E. Bathen, U. Grossner, Energy-dependent impact of proton irradiation on 4H-SiC schottky diodes, Mater. Sci. Forum 1092 (2023) 187–192, http://dx.doi.org/10.4028/p-0y444y, Publisher: Trans Tech Publications Ltd. URL: https://www.scientific.net/MSF.1092.187.

[29] T. Hornos, A. Gali, B.G. Svensson, Large-scale electronic structure calculations of vacancies in 4H-SiC using the heyd-scuseria-ernzerhof screened hybrid density functional, Mater. Sci. Forum 679–680 (2011) 261–264, http://dx.doi.org/10.4028/www.scientific.net/MSF.679-680.261, URL: https://www.scientific.net/MSF.679-680.261.

[30] N.T. Son, X.T. Trinh, L.S. Løvlie, B.G. Svensson, K. Kawahara, J. Suda, T. Kimoto, T. Umeda, J. Isoya, T. Makino, T. Ohshima, E. Janzén, Negative-u system of carbon vacancy in 4 H -SiC, Phys. Rev. Lett. 109 (18) (2012) 187603, http://dx.doi.org/10.1103/PhysRevLett.109.187603, URL: https://link.aps.org/doi/10.1103/PhysRevLett.109.187603.

[31] T. Dalibor, G. Pensl, H. Matsunami, T. Kimoto, W.J. Choyke, A. Schöner, N. Nordell, Deep defect centers in silicon carbide monitored with deep level transient spectroscopy, Phys. Status Solidi (a) 162 (1) (1997) 199–225, http://dx.doi.org/10.1002/1521-396X(199707)162:1<199::AID-PSSA199>3.0.CO;2-0, URL: https://onlinelibrary.wiley.com/doi/abs/10.1002/1521-396X%28199707%29162%3A1%3C199%3A%3AID-PSSA199%3E3.0.CO%3B2-0.

[32] L. Storasta, H. Tsuchida, T. Miyazawa, T. Ohshima, Enhanced annealing of the Z1/2 defect in 4H–SiC epilayers, J. Appl. Phys. 103 (1) (2008) 013705, http://dx.doi.org/10.1063/1.2829776, URL: http://aip.scitation.org/doi/10.1063/1.2829776.

[33] K. Kawahara, J. Suda, T. Kimoto, Analytical model for reduction of deep levels in SiC by thermal oxidation, J. Appl. Phys. 111 (5) (2012) 053710, http://dx.doi.org/10.1063/1.3692766, URL: http://aip.scitation.org/doi/10.1063/1.3692766.

[34] T. Okuda, G. Alfieri, T. Kimoto, J. Suda, Oxidation-induced majority and minority carrier traps in n- and p-type 4H-SiC, Appl. Phys. Express 8 (11) (2015) 111301, http://dx.doi.org/10.7567/APEX.8.111301, URL: https://iopscience.iop.org/article/10.7567/APEX.8.111301.

[35] H. Wu, G. Sun, T. Yang, G. Yan, L. Wang, W. Zhao, X. Liu, Y. Zeng, J. Wen, Effect of annealing process on the surface roughness in multiple Al implanted 4H-SiC, J. Semiconductors 32 (7) (2011) 072002, http://dx.doi.org/10.1088/1674-4926/32/7/072002, URL: https://iopscience.iop.org/article/10.1088/1674-4926/32/7/072002.

[36] I. Capan, T. Brodar, Majority and minority charge carrier traps in n-Type 4H-SiC studied by junction spectroscopy techniques, Electron. Mater. 3 (1) (2022) 115–123, http://dx.doi.org/10.3390/electronicmat3010011, URL: https://www.mdpi.com/2673-3978/3/1/11.

[37] I. Capan, Y. Yamazaki, Y. Oki, T. Brodar, T. Makino, T. Ohshima, Minority carrier trap in n-type 4H–SiC Schottky barrier diodes, Crystals 9 (7) (2019) 328, http://dx.doi.org/10.3390/cryst9070328, URL: https://www.mdpi.com/2073-4352/9/7/328.

[38] H.M. Ayedh, V. Bobal, R. Nipoti, A. Hallén, B.G. Svensson, Formation of carbon vacancy in 4H silicon carbide during high-temperature processing, J. Appl. Phys. 115 (1) (2014) 012005, http://dx.doi.org/10.1063/1.4837996, URL: https://pubs.aip.org/jap/article/115/1/012005/139004/Formation-of-carbon-vacancy-in-4H-silicon-carbide.

[39] J. Coutinho, Theory of the thermal stability of silicon vacancies and interstitials in 4H–SiC, Crystals 11 (2) (2021) 167, http://dx.doi.org/10.3390/cryst11020167, URL: https://www.mdpi.com/2073-4352/11/2/167.

[40] N. Für, M. Belanche, C. Martinella, P. Kumar, M.E. Bathen, U. Grossner, Investigation of electrically active defects in SiC power diodes caused by heavy ion irradiation, IEEE Trans. Nucl. Sci. (2023) 1, http://dx.doi.org/10.1109/TNS.2023.3242760, Conference Name: IEEE Transactions on Nuclear Science.

[41] I.G. Ivanov, A. Henry, E. Janzén, Ionization energies of phosphorus and nitrogen donors and aluminum acceptors in 4 h silicon carbide from the donor-acceptor pair emission, Phys. Rev. B 71 (24) (2005) 241201, http://dx.doi.org/10.1103/PhysRevB.71.241201, URL: https://link.aps.org/doi/10.1103/PhysRevB.71.241201.

[42] H.J. Von Bardeleben, J.L. Cantin, L. Henry, M.F. Barthe, Vacancy defects in *p* -type 6 H - SiC created by low-energy electron irradiation, Phys. Rev. B 62 (16) (2000) 10841–10846, http://dx.doi.org/10.1103/PhysRevB.62.10841, URL: https://link.aps.org/doi/10.1103/PhysRevB.62.10841.

[43] T. Kimoto, K. Kawahara, B. Zippelius, E. Saito, J. Suda, Control of carbon vacancy in SiC toward ultrahigh-voltage power devices, Superlattices Microstruct. 99 (2016) 151–157, http://dx.doi.org/10.1016/j.spmi.2016.03.029, URL: https://linkinghub.elsevier.com/retrieve/pii/S0749603616301239.

[44] T. Hiyoshi, T. Kimoto, Reduction of deep levels and improvement of carrier lifetime in n-type 4H-SiC by thermal oxidation, Appl. Phys. Express 2 (2009) 041101, http://dx.doi.org/10.1143/APEX.2.041101, URL: https://iopscience.iop.org/article/10.1143/APEX.2.041101.